Acoustic signature analysis of the interaction between a dc plasma jet and a suspension liquid jet

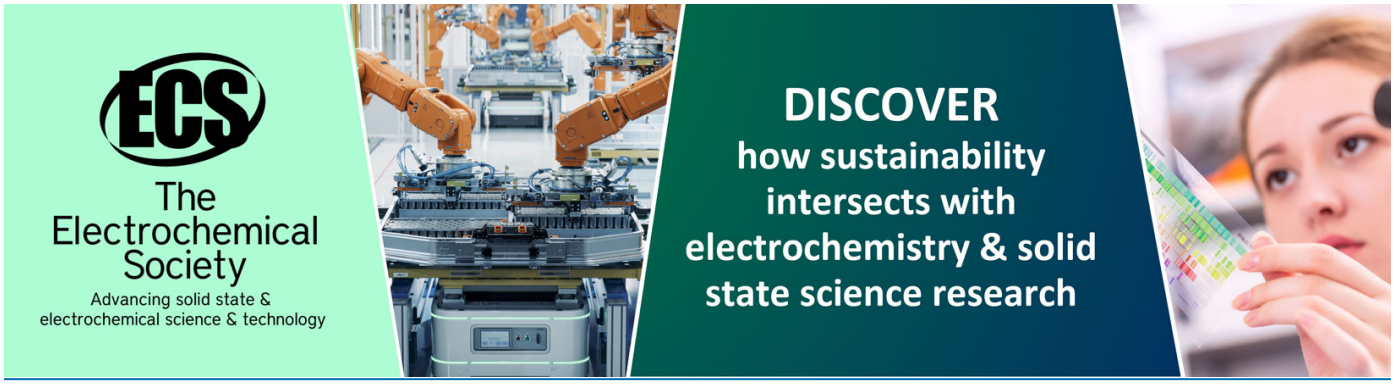

J. Phys. D: Appl. Phys. **42** (2009) 195202 (12pp) doi:10.1088/0022-3727/42/19/195202

Acoustic signature analysis of the interaction between a dc plasma jet and a suspension liquid jet

V Rat and J F Coudert

SPCTS-CNRS UMR 6638, University of Limoges, 123 av. A Thomas 87060 Limoges cedex, France

Received 21 April 2009, in final form 21 July 2009
Published 18 September 2009
Online at stacks.iop.org/JPhysD/42/195202

Abstract

Suspension plasma spraying allows forming finely structured coatings by injecting suspensions of ceramic particles within a dc plasma jet. The electric arc motion in dc plasma torch is the main acoustic source which is modified by the injection of suspension. The analyses of cross-correlations between the arc voltage and the acoustic signal show a decrease in time propagations due to local cooling of the plasma jet when injecting suspensions. Moreover, power spectra highlight acoustic amplifications below a certain frequency threshold and attenuations above. A simplified model of the frequency acoustic response of a two-phase vaporizing mixture is used to interpret experimental measurements. These acoustic effects are due to the dynamics of thermal transfers between vaporizing liquid and plasma.

(Some figures in this article are in colour only in the electronic version)

Nomenclature

c	sound velocity (m s^{-1})
c_ℓ	liquid specific heat (J kg^{-1} K^{-1})
c_p	plasma specific heat (J kg^{-1} K^{-1})
d	droplet diameter (m)
f	frequency (Hz)
h_0	mean specific enthalpy (J kg^{-1})
I	arc current (A)
k	phase mass ratio (ρ_p/ρ)
L_v	latent heat of vaporization (J kg^{-1})
$\dot{m}_g$	gas mass flow rate (kg s^{-1})
M_g	mass of plasma phase (kg)
M_p	mass of droplet phase (kg)
n	droplet number
N	response factor
N_p	droplet number per unit volume (m^{-3})
p	pressure (Pa)
p_0	mean pressure (Pa)
p'	acoustic pressure (Pa)
p_v	saturation vapour pressure (Pa)
Q_v	convective power per volume unit (W m^{-3})
T	mean plasma temperature (K)
T_p	mean droplet phase temperature (K)
V	arc voltage (V)
V_g	volume of plasma phase (m^3)
V_p	volume of droplet phase (m^3)
V_m	volume of plasma and droplet phases ($V_g + V_p$) (m^3)
w	vaporization rate per volume unit (kg s^{-1} m^{-3})
W_0	total electric power (W)
γ	isentropic exponent
κ	plasma thermal conductivity (W m^{-1} K^{-1})
ρ	mass concentration of plasma phase (kg m^{-3})
ρ_ℓ	density of liquid (kg m^{-3})
ρ_p	mass concentration of droplet phase (kg m^{-3})
τ_v	characteristic time of vaporization (s)
Φ_{th}	electrode thermal heat losses (W)
ω	angular frequency (rad s^{-1})

1. Introduction

For the last decade many research efforts have been focused on the development of elaboration techniques of nanostructured ceramics coatings with intermediate thicknesses (2–50 μm) for solid oxide fuel cell components, wear resistance or photo-catalytic applications, thermal barrier coatings [1]. The use of thermal plasma sources in solution precursor plasma spraying (SPPS) or in suspension plasma spraying (SPS) presents unique advantages because they involve high levels of specific

enthalpy and momentum allowing efficient thermal, reactive and dynamic treatments of solid or liquid precursors.

In both processes, liquid and solid precursors are injected within a dc plasma jet, are plasma-treated and sprayed onto a prepared substrate to form finely structured coatings. The main similarity between SPPS and SPS can be ascribed to the liquid injection mode in the plasma. This is because submicrometre solid particles must be injected to form nanostructured coatings and, due to their low inertia, they require a liquid carrier to bring them in the core of the plasma jet. In SPPS, a fully liquid precursor is injected and vaporization processes favour the formation of solid precipitates which are plasma sprayed. In the case of SPS, a suspension is injected and consists of a solvent in which submicrometre ceramic particles are dispersed by using a dispersant. The latter allows adsorbing at the solid particles surface polymeric chains which exert electrostatic and steric repulsions between solid particles, avoiding their agglomeration.

Precursors are injected as droplet clouds in SPPS or by using a liquid jet (continuous or not) in SPS whose diameter is about 300 μm. In the latter case, the plasma/liquid jet interaction first produces a primary fragmentation resulting in droplet size distribution within the plasma, and liquid vaporization processes arise later.

The fragmentation and vaporization processes completely govern the particle trajectories in the plasma plume further downstream from the nozzle exit [2]. That is why it is particularly important to control the liquid injection and its interaction with the plasma jet. It is indeed well known that the dc plasma torch produces strong arc instabilities and a slow decrease in the energetic performance of the plasma torch due to erosion electrode phenomena.

Hence, depending on their size and trajectories, the particles experience different thermal histories and trajectories leading to different molten states and impact location onto the substrate. Depending upon the fraction of poorly treated particles (processed or re-solidified in the plasma jet core fringes) to the one appropriately treated (processed in the plasma core and in a molten state when impacting), the coating architecture will evolve from fairly dense (low fraction of poorly treated) to fairly porous (high fraction of poorly treated).

In general, the conventional diagnostic techniques are not suited to investigate the plasma/precursor interaction. For example, the optical emission spectroscopy technique must tackle not only the problem of the assumption regarding the non-local thermodynamical equilibrium due to vaporization and also the Abel inversion which cannot be applied due to the asymmetry of the plasma jet when injecting [3]. Moreover, in SPS, the number of solid particles injected per time unit can reach 10^9 s^{-1}. Consequently, diagnostic techniques (e.g. laser anemometry) based on the diagnostic of one particle to obtain velocity or temperature cannot be used due to the particle size and their flow rate. Furthermore, other techniques based on cross-correlations of light signals emitted by particles recorded at two distinct locations cannot be obtained with accuracy if these measurements are performed within the plasma plume. In general, for example in SPS, the range of interest corresponds to the first tens of millimetres in the plasma plume.

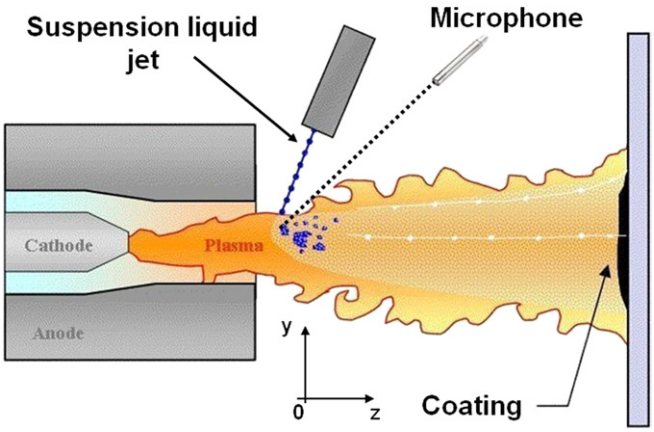

Figure 1. SPS and microphone positioning.

In this paper, we use acoustic diagnostics to investigate the suspension/plasma interaction. The sources of acoustic emissions generated by electric arcs were studied by Fitaire [4] and Dadgar [5]. Sound refraction from dc plasma torches was highlighted by Pauvit *et al* [6] and acoustic diagnostics were used by Badie *et al* [7] to study the turbulent transition of the dc plasma jet.

This paper presents, to our knowledge, the first report concerning the acoustic response of a dc plasma jet to the injection of a suspension of submicrometre particles. A physical interpretation of the observed phenomena is proposed and also an on-line control method of the quality injection in the SPS process. Section 2 presents experimental facilities and procedures. Section 3 shows the acoustic signature of the suspension/plasma jet interaction. Section 4 presents a simplified analytical model to interpret measurements.

2. Experimental descriptions

2.1. Dc plasma torch

A dc commercial (SMF4) plasma torch is power supplied with a current regulated source and the gas feeding rate is controlled with a mass flow meter. The process is depicted in figure 1. The input parameters are the arc current, I, the gas mass flow rate, $\dot{m}_g$ and the gas composition. The dependent, or output, parameters are the arc voltage, V, and the heat losses to the electrodes, Φ_{th}.

Measurements of V, I and Φ_{th} allow characterizing the plasma torch [8], i.e. determining a mean effective specific enthalpy of the plasma jet h_0 such that $h_0 = (VI - \Phi_{th})/\dot{m}_g$.

A digital multimeter successively samples at 50 Hz with an accuracy of 16 bits three channels corresponding to the arc voltage V through a dividing voltage bridge, the arc current I by using a shunt resistance and the electrode thermal losses. The latter are deduced from calorimetric measurements performed on the water cooling system of the plasma torch. A procedure of double averaging on each measurement during approximately 1 min allows the determination of a reliable mean experimental value. The multimeter is controlled via a GPIB card by Labview software.

Pure argon as plasma gas is used in this study and a mixture of Ar–H_2 as well. These plasma gases are widely used in plasma spraying because of the properties of momentum transfers for pure argon and of thermal transfers for hydrogen. The addition of hydrogen leads to an increase in the electric field of the column arc and consequently in the mean arc voltage. This is mainly due to the dissociation of hydrogen molecules which increases thermal radial losses compensated by the increase in the Joule heating source (σE^2, where σ and E are the electrical conductivity and the electric field of the arc column) to ensure the arc current flow. The power dissipated increases in the plasma and heat losses to the electrode as well. The net power available in the plasma jet is, however, increased since the mean specific enthalpy is higher for the Ar–H_2 mixture than for pure argon as shown in table 1 which reports the plasma torch operating parameters. The influence of both plasma mixtures is investigated because a more efficient vaporizing effect is expected in the case of Ar–H_2 and therefore an acoustical response different from that of pure argon.

2.2. Suspensions and their injection in plasma

Suspensions are composed of α-Al_2O_3 powder (see table 2 for size distribution) dispersed within pure ethanol by using a phosphate ester as dispersant (1 wt% of powder).

The mass load of powder is 10 wt% of ethanol. Suspensions are stored within air pressurized tanks and injected through a circular diaphragm (150 μm in diameter) into the plasma jet by applying an air injection pressure varying from 0.4 to 0.6 MPa.

Figure 2 depicts a time-resolved image of suspension injection within an Ar–H_2 (45–15 slm) plasma jet operating at 500 A. This picture was acquired by using synchronized laser illumination and a camera aperture with a voltage level of 65 V. This voltage corresponds to the mean voltage. Details regarding this method were given in [2].

This figure shows that the liquid jet starts to be destabilized by natural fragmentation outside the plasma because droplet formation is observed. Then, inside the plasma jet, liquid jet is fragmented at the necks of the liquid jet instabilities. Further downstream droplets are fragmented, accelerated, heated and vaporized. Solid particles contained within these droplets also undergo acceleration, heating and melting.

Liquid jet velocities outside the plasma jet were measured as a function of injection pressure used in the frame of this paper, namely at 0.4 and 0.6 MPa. With the same time-resolved imaging system as above, drops were illuminated with two laser pulses whose time gap is known. Consequently, from the analysis of pictures, drop velocities are deduced. Table 2 reports the results of the measurements and the corresponding suspension mass flow rate. Moreover, the mean distance between drops in the liquid jet is found to be 730 $\pm$ 60 μm. The drop injection frequency within the plasma jet can be estimated to range between 35 and 50 kHz.

Table 1. Plasma torch parameters.

Plasma gas	Ar–H_2 (45–15 slm)	Ar (45 slm)
Mean torch voltage (V)	69.90	37.30
Arc current (A)	507.80	502.00
Heat losses Φ_{th} (kW)	13.30	7.57
Mass flow rate (g s^{-1})	1.36	1.34
Mean specific enthalpy h_0 (MJ kg^{-1})	16.32	8.32

2.3. Acoustics measurements

Acoustics measurements are performed by using a free-field 1/4′ microphone (type 4954 Bruel & Kjær, 100 kHz bandwidth). Previous acoustic studies have shown that dc plasma torches produce acoustical emissions [6, 7] out of a conical axial zone (silent cone) from the nozzle exit. This is due to flow velocity and sound velocity gradients between the plasma jet and surrounding air. The conservation of the axial velocity component between each region with different flows and sound velocities causes curvature of acoustic rays [9].

The microphone sensor is therefore positioned out the silent cone at 70 mm from the point defined by the axis of the plasma torch and its perpendicular plane in the nozzle exit. Moreover, the microphone direction is located in the plane defined by the torch axis and the suspension injection direction. The angle between the axis of the plasma torch and the microphone direction is 45°. This positioning is important because the microphone directly detects sound emission coming from the interaction volume. Figure 1 shows the SPS process and the microphone positioning.

Previous works have shown that characteristic times of fragmentation processes of liquid are much lower than those of liquid vaporization [3]. The characteristic times of fragmentation are about 1 μs or below and it is then expected that the microphone cannot detect the fragmentation processes because of the frequency bandwidth of the microphone.

Moreover, it has also been shown when performing optical emission spectroscopy [3] on oxygen atomic lines from water injected as solvent for suspensions that, 15 mm

Table 2. Suspensions liquid jet parameters.

Powder size distribution in number (μm)	$d_{10} = 0.04$, $d_{50} = 0.52$, $d_{90} = 1.31$	
Powder load (wt% of ethanol)	10%	
Dispersant (wt% of powder)	1%	
Injection pressure (MPa)	0.4	0.6
Drops velocity (m s^{-1})	26.6	33.5
Suspension mass flow rate (g s^{-1})	0.38	0.47

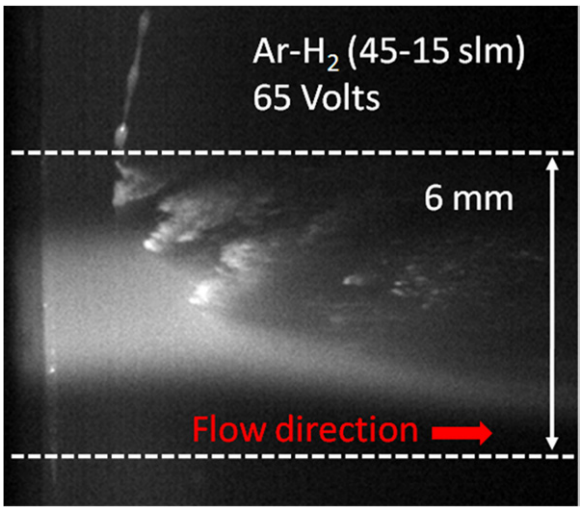

Figure 2. Time-resolved image of the injection in SPS. Time aperture of 10 μs synchronized with the instantaneous voltage level of 65 V. Ar–H_2 (45–15 slm), 500 A, internal nozzle diameter of 6 mm.

downstream of the nozzle exit, the mixture of plasma and water is homogeneous. This means that liquid vaporization is completed. Since suspensions are injected 2 mm downstream of the nozzle exit, the interaction volume V_i is about 368 mm^3, with an internal anode nozzle diameter of 6 mm. The microphone being positioned at a distance L of 70 mm from the nozzle exit (see section 2.3), we check $\sqrt[3]{V_i} \ll L$. It is then supposed that the interaction volume is a source point.

In the case of ethanol as solvent in this paper, it is expected that this volume interaction is smaller because ethanol has lower vaporization enthalpy, boiling temperature and specific heat than water.

Cross-correlations between the arc voltage and the acoustic signals as well as power spectra are calculated from time-resolved signals. The latter are measured with 14 bits of accuracy by using a simultaneous data acquisition PCI computer card piloted by Labview software. Signals are sampled at 100 kHz during 0.2 s (i.e. 5 Hz frequency resolution). The sampling rate corresponds to the maximum of microphone frequency bandwidth which allows a maximum frequency f_{max} of 50 kHz.

In order to compare spectra obtained under different experimental conditions, the power spectra were normalized with respect to the variance of the voltage. The instantaneous voltage, $U(t)$, is the sum of the mean value, V, and of the fluctuating component, $v(t)$. The average squared quantities are linked so that

$$\langle U^2 \rangle = V^2 + \langle v^2 \rangle, \tag{1}$$

where the last term, $\langle v^2 \rangle$, is the variance of the voltage. The power spectrum, $\Phi_v(f)$, of the voltage fluctuating component, $v(t)$, that is the squared amplitude of its Fourier components, is such that

$$\int_0^{f_{max}} \Phi_v(f) \mathrm{d}f = \langle v^2 \rangle. \tag{2}$$

Before normalization, a central moving average of power spectra is performed for 100 data points. This procedure does not modify the variance of the signal.

3. Acoustic emissions

Without igniting plasma, the plasma torch used in this study produces an acoustic emission (whistling) when plasma gas is flowing. It has been shown that the whistling frequency is linearly dependent on the gas volume flow rate and corresponds to the Kármán vortex street [10].

When igniting plasma, the Kármán vortices disappear and the main origin of acoustic emission is related to the electric arc and its motion inside the torch nozzle as explained below.

3.1. Fitaire law

The origin of acoustic emission in weakly ionized gases is attributed to the kinetic energy transfers from electrons accelerated in the electric field to neutral gas. It has been shown that the time variation of the rate of energy absorbed by the electrons per unit volume is a source term of the propagation equation of sound pressure [9]. In particular, Fitaire [4] showed that this source term is proportional to $\partial W/\partial t$ where W is the power supplied to electrons through an external electric field. Later, Dadgar showed that, in the case of transferred electric arcs, the acoustic amplitude from the electric arc is proportional to the time variation of the electrical power supplied to the arc [5]:

$$a(t) \propto \frac{\gamma - 1}{c^2} \frac{\partial W_0}{\partial t}, \tag{3}$$

where $a(t)$ is the instantaneous acoustic amplitude, W_0 is the total electrical power and γ and c, respectively, the isentropic exponent and sound velocity.

The Fitaire law (equation (3)) shows that acoustic amplitude and the arc torch voltage are correlated, the arc current being maintained constant during experiments.

In the case of a blown arc, involved in SPS, equation (3) must be valid.

Sound emission and the arc torch voltage as well have been simultaneously recorded, as explained in section 2.3, in order to validate not only the Fitaire law but also the experimental protocol of sound recording.

Figure 3 depicts the time dependence of the arc voltage and the integral of the acoustic signal recorded by the microphone for an Ar–H_2 mixture (see table 1). It allows checking the integration of equation (3). The integration of equation (3) has been preferred rather than its derivation to limit the influence of numerical noise.

It is checked that the arc voltage and the acoustic signal are linked following equation (3). This means that the electric arc motion within the anode nozzle is the acoustic source because the arc length variations entail power supplied variations at constant arc current transmitted to the plasma gas.

It has to be noted that in figure 3 the acoustic signal has been time shifted to be in phase with the arc voltage. This shift is due to the sound propagation delay from the nozzle exit to the microphone and the phase shift due to the integration of equation (3) by $(-T/4)$ where T is the signal period.

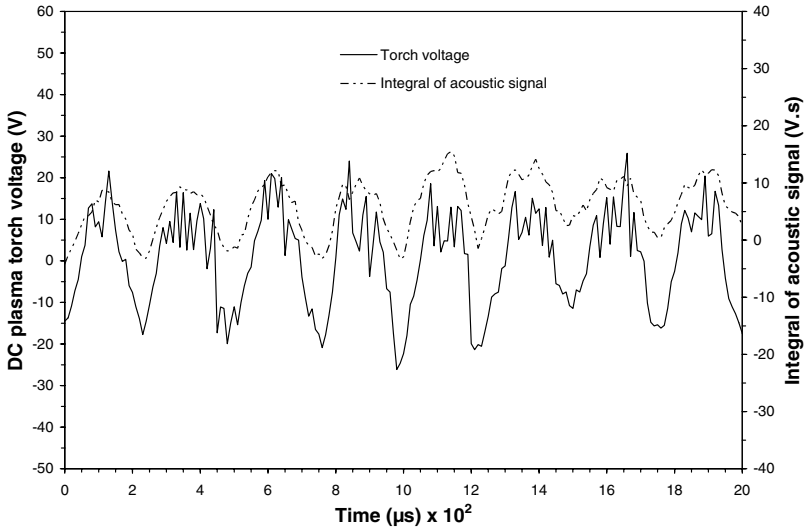

Figure 3. Time dependence of the arc torch voltage and the integral of acoustic signal of a blown electric arc Ar–H_2 (45–15 slm) (see table 1).

3.2. Correlation between the torch voltage and acoustics signal

As previously explained, the arc voltage time variations are an acoustical source and, consequently, the arc torch voltage signal should be correlated with the acoustical one. With the use of the operating parameters in this study, it has been recently shown that dc plasma torches can behave like a Helmholtz acoustical resonator [10, 11]. The arc voltage fluctuations are coupled to pressure oscillations of plasma gas in the cathode cavity, in the rear part of the plasma torch.

Figure 4(*a*) depicts the raw power spectrum of the torch voltage signal operating at 500 A, Ar–H_2 (45–15 slm) without suspension injection.

In general, the presence of narrow peaks in the power spectrum means that resonance phenomena occur in the plasma torch. A quality factor can then be associated with each peak which depends on irreversible effects such as viscosity dissipation, turbulence, head losses due to the anode/cathode position and also on operating parameters. For example, the works of Kavka *et al* [12] have shown that the relative position of the cathode/anode influences the power spectrum of the arc voltage.

The first peak is always present in the range 4–5 kHz and is generally the most important. It is clearly identified as a Helmholtz resonance mode [10]. The amplitude of this mode is quite sensitive to operating conditions. The volume of the cathode cavity particularly affects the amplitude and the width of the Helmholtz peak [10].

The other peak has (around 7 kHz) an unclear origin which probably corresponds to another resonance mode of the cathode cavity. The remaining spectrum is attributed to the restrike mode which is a phenomenon more distributed in frequency as shown in the inset of figure 4(*a*).

Figure 4(*b*) depicts the normalized power spectrum of the torch voltage signal operating at 500 A, Ar–H_2 (45–15 slm) without suspension injection (0 bar) and with suspension injection at 4 and 6 bar.

This procedure flattens the weak components occurring at higher frequencies but this representation was chosen to highlight the effect of injection on the voltage power spectrum.

It is interesting to observe that the injection of suspension at the nozzle exit influences the arc voltage since the amplitude of major and minor peaks of the power spectrum, respectively, increases and decreases. The flow regime being subsonic, the pressure perturbations caused by the suspension injection (see section 4) propagate upstream and slightly modify the acoustical resonance of the cathode cavity.

Without injection, this main voltage fluctuation (or related main pressure oscillation) causes an acoustic emission which propagates within the plasma jet and is recorded by the microphone. Figure 3 has shown the correlation between voltage and acoustical pressure through the Fitaire law. The acoustic and voltage signals are also time correlated due to the sound propagation. The latter occurs in the plasma jet and also in the air surrounding the plasma jet up to the microphone. The sound velocity c_0 depends mainly on the local temperature ($c_0 \propto \sqrt{T}$) and it is about one order of magnitude higher in the plasma jet than in air, 3000 m s^{-1} in plasma against about 350 m s^{-1} in air. The distance between the cathode tip and the nozzle exit is around 30 mm and that of the plasma exit and the microphone 70 mm. Therefore, the propagation time in the plasma is about 10 and 200 μs in air. Because of the temperature dependence of sound velocity, the propagation time should be modified due to suspension injection since the latter causes a local cooling of the plasma jet due to vaporization processes.

According to the Fitaire law, this propagation time can be evaluated from the simultaneous measurements of the arc voltage and the acoustical signal by calculating the cross-correlations of both signals. However, as suggested in figure 2, the plasma fluctuations at the nozzle exit entail non-uniform drops fragmentation and vaporization processes. Consequently, weak variations in time propagations due to suspension injection and plasma fluctuations can be expected. Thus, to obtain a statistical repartition of propagation times, cross-correlations of arc voltage and the integral of acoustical

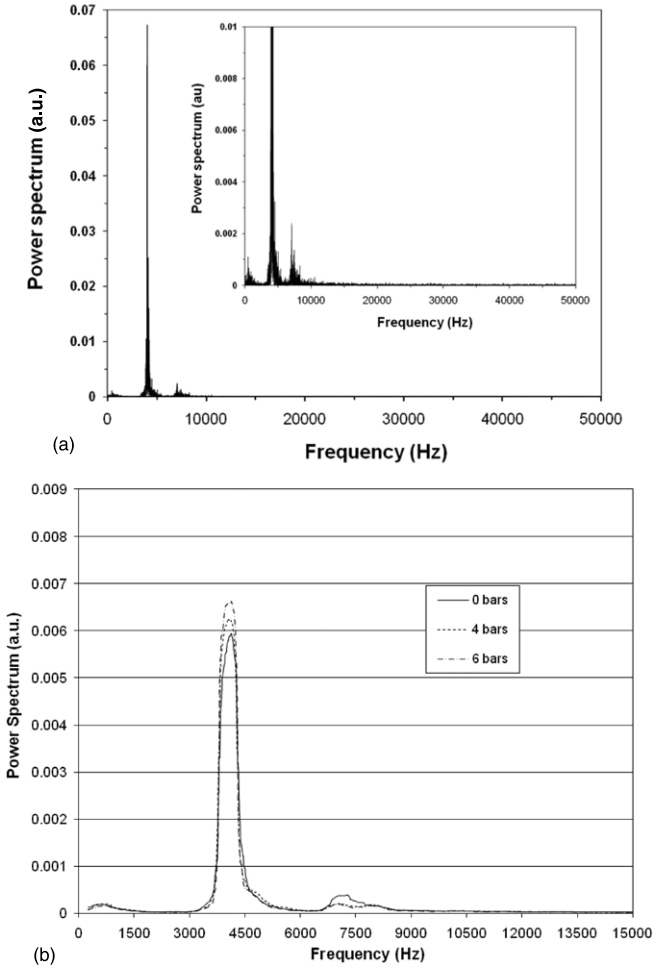

Figure 4. Power spectrum of the torch voltage signals operating at 500 A, Ar–H_2 (45–15 slm): (*a*) without suspension injection (0 bar); (*b*) without and with suspension injection at 4 and 6 bar. Inset of (*a*) shows power spectrum at lower scale. (*a*) depicts raw measurements, and in (*b*), spectra are smoothed by the use of central moving average and normalized.

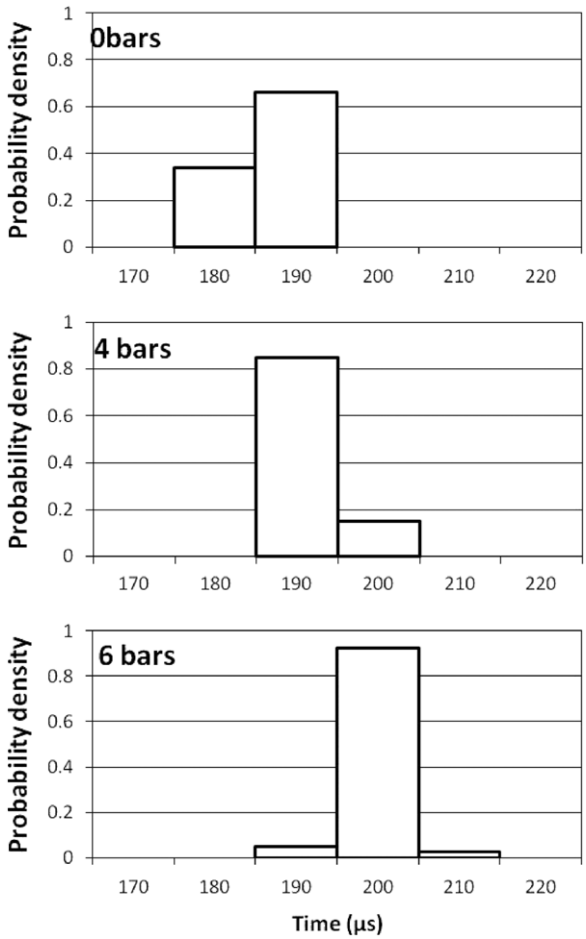

Figure 5. Histograms of measured propagation times of acoustic signals without suspension injection (0 bar) and with suspension injection at 4 and 6 bar—Ar–H_2 (45–15 slm)—500 A.

signals (the Fitaire law) were calculated. More than 100 propagation times were taken into account. Signals were sampled at 100 kHz during 20 ms. The maximum positions in cross-correlation functions give time propagations and are gathered together in a histogram giving the probability density.

Figure 5 presents histograms of measured propagation times of acoustic signals without suspension injection (0 bar) and with suspension injection at 4 and 6 bar for an Ar–H_2 (45–15 slm) plasma operating at 500 A (see table 1). It can be observed that the absolute values of propagation times are consistent with the microphone position and the estimated sound velocity. The latter continuously varies within the plasma and in the surrounding air. Despite the limited bandwidth of the microphone (100 kHz), a shift to the higher propagation times can be distinguished when increasing the pressure injection. Note that increasing the latter is equivalent to increasing the suspension mass flow rate (see table 2). This means that the liquid mass per time unit to be vaporized increases as the injection pressure increases. It can then be assumed that the local temperature decreases [3], which in turn reduces the sound velocity, and increases the sound propagation time.

3.3. Power spectrum of acoustic signals

The origin of acoustic emissions when injecting suspension within a thermal plasma jet is of prime importance in understanding the involved phenomena. As shown above, the plasma jet itself produces sounds due to voltage fluctuations. Moreover, each process involving transient transfers in mass, momentum and energy should participate in creating sound emission. The air engulfment downstream from the plasma jet also produces sound emission due to turbulence [7]. Consequently, since suspension drops are injected with a frequency between 35 and 50 kHz, the power spectrum should highlight this injection frequency. It will be shown that the microphone does not detect this drops emission frequency, either because of too low microphone sensitivity or because the drop injection frequency is not accurately defined and is distributed in a wide frequency range.

Moreover, the fragmentation phenomena which correspond to sudden momentum transfers between the plasma and the drops present characteristic times below 10 μs [3]. Consequently, the microphone will not detect the fragmentation

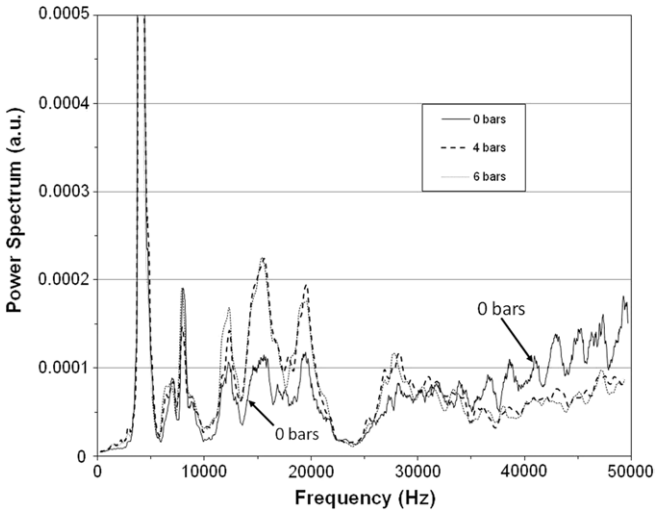

Figure 6. Power spectra of acoustic signals generated at 500 A, Ar–H_2 (45–15 slm) without suspension injection (0 bar) and with suspension injection (injection pressure: 4 and 6 bar).

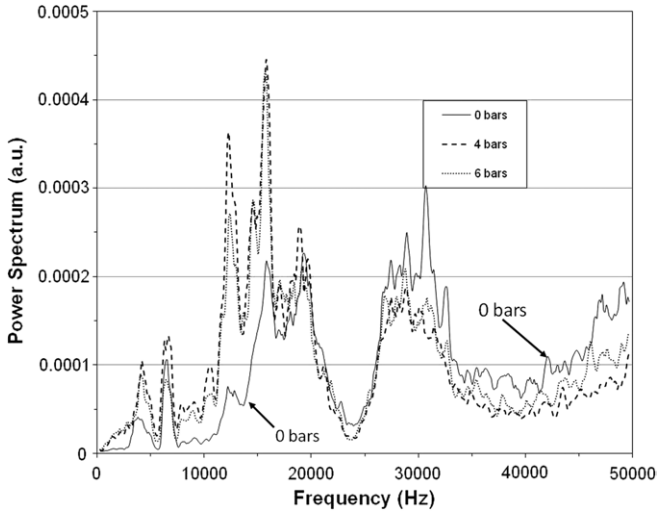

Figure 7. Power spectra of acoustic signals generated at 500 A, Ar (45 slm) without suspension injection (0 bar) and with suspension injection (injection pressure: 4 and 6 bar).

processes of individual drops due to a low microphone frequency bandwidth. Finally, heat transfers from plasma to drops have characteristic times higher than fragmentation ones, depending on the local plasma jet thermo-physical properties. As shown below, the analyses of the power spectrum of acoustic signals highlight the interaction between drops and plasma due to liquid vaporization.

Figure 6 presents the power spectra of the acoustic signal (500 A, Ar–H_2 (45–15 slm)) without suspension injection (0 bar) and with suspension injection (4 and 6 bar). Without injection, the major peak (∼4000 Hz) corresponds to that of the arc voltage power spectrum (see figure 4). At higher frequencies and 0 bar, a progressive increase in the amplitude is observed. This is linked to the Fitaire law where $a(t) \propto \partial V/\partial t$ ($a(t)$ and V are, respectively, the acoustical and voltage signals). In the Fourier representation, $\Phi_a(f) \propto f^2\Phi_v(f)$ where $\Phi_a(f)$ is the power spectrum of $a(t)$. The high frequency components of $\Phi_v(f)$ are increased in $\Phi_a(f)$ due to the quadratic term of frequency.

Power spectra in figure 6 also show that the injection of suspensions does not create any new frequency components, but contributes to amplify below 32 kHz and to attenuate above 32 kHz the existing frequency components generated by the plasma itself. The maximum of amplification is observed around 15 kHz.

This means that the occurrence of other frequency contributions in power spectra of the arc voltage when changing the operating parameters will be amplified or attenuated, depending on the frequency, in power spectra of sound signal.

Figure 7 depicts the power spectra of the acoustic signal generated at 500 A with pure argon plasma (45 slm) without suspension injection (0 bar) and with suspension injection (4 and 6 bar). The same behaviour is observed with pure argon as with Ar–H_2 mixture. The effect of acoustic amplification is observed below 20 kHz and the attenuation above. The maximum of amplification is around 12 kHz.

For both plasma compositions (pure argon and Ar–H_2), acoustic waves produced by the plasma are amplified below a certain threshold and are damped above. This transition is observed at lower frequency for pure argon than for Ar–H_2.

4. Discussion

The physical interpretation of this sound emission is delicate because of the complexity of the plasma medium which is highly inhomogeneous and dissipative. It is out of the scope of this paper to model the sound emission due to plasma/suspension interaction. Instead, a semi-quantitative approach is preferred to physically interpret sound attenuation or amplification effects. The following discussion is based on pioneering works of Heidmann and Wieber (HW) [13] regarding acoustic mode instability in a rocket engine combustor. They indeed observed attenuation and amplification of sound due to propellant vaporization. The acoustic amplification can lead to unstable combustion for which many efforts are produced [14] to control damping or driving mechanisms of acoustic instabilities.

Establishing simplified mass and energy conservation equations of a droplet immersed in a uniform and steady hot gas, they studied the variation of the droplet vaporization rate (kg s^{-1}) due to the acoustic pressure in a linear approximation. The droplet mass and energy equations are linearized because acoustic perturbations are weak with respect to ambient pressure. The pressure p can be written as $p = p_0 + \tilde{p}'$, where p_0 and $\tilde{p}'$ are, respectively, the mean value and the acoustic pressure. This acoustic perturbation is therefore superimposed on the unperturbed behaviour of the droplet and can modify the heat and mass transfers.

Heidmann and Wieber defined the acoustic response (response factor, N) of such a system.

The response factor is based upon the Rayleigh criterion [15] which states that acoustic amplification occurs if energy (or mass) is added to the propagating acoustic wave when

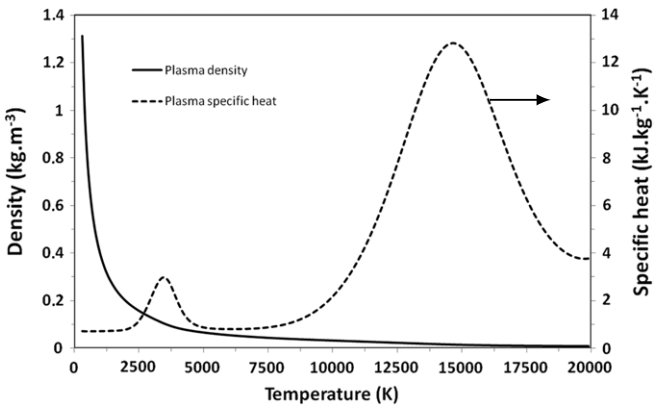

Figure 8. Temperature dependence of density and specific heat of Ar–H_2 (75 mol%Ar) plasma at atmospheric pressure [16].

pressure is above its mean value. Conversely, attenuation occurs when mass is added when pressure is below its mean value. As shown below, the calculation of the response factor roughly consists of evaluating the product $\tilde{p}' \cdot \tilde{w}'$, where $\tilde{w}'$ is the perturbation of the vaporization rate due to $\tilde{p}'$.

However, the HW model does not consider the variations of the local thermal properties (temperature, specific heat, density) which are known to be very important in thermal plasmas. For example, figure 8 shows the temperature dependence of density and specific heat of an Ar–H_2 (75 mol%Ar) thermal plasma calculated at atmospheric pressure [16]. The plasma density is seen to decrease as temperature increases and specific heat as a function of temperature shows strong non-linear behaviour. The low temperature peak corresponds to hydrogen molecules dissociation whereas the higher temperature peak accounts for ionization reactions of argon and hydrogen atoms.

Moreover, the HW model does not consider the mass and energy conservation equations of heating gas. Finally, as shown below, the frequency positive response according to the HW model presents a width which is much higher than that obtained in the experimental study.

Consequently, a model similar to that of HW is proposed in the next section, where mass and energy conservation equations of the plasma are considered. The frequency response of a two-phase vaporizing mixture consisting of a plasma phase and a droplet phase is derived.

4.1. Simplified model of frequency acoustic response of a two-phase vaporizing mixture

The arc generated plasma volume and its mass are, respectively, V_g and M_g. A phase consisting of n droplets with a diameter d, each with a density ρ_ℓ, occupies an overall volume V_p and a mass M_p, and is being vaporized by a plasma. In the interaction volume detected by the microphone, the number of droplets per unit volume is $N_p = n/V_m$, where V_m is the volume of the mixture, i.e. $V_m = V_p + V_g$, and is assumed to be constant. This assumption is justified by the fact that characteristic times of droplet fragmentation are much lower than those of vaporization [3], hence vaporization starts after the fragmentation processes. The volume V_m corresponds to the volume interaction between the plasma and the droplets where secondary fragmentation can be neglected, i.e. the darkened region on the right-hand side of figure 2.

The droplet number entering the volume, due to fragmentation, is supposed to be equal to the droplet number leaving the interaction volume due to vaporization.

The plasma gas is an argon–hydrogen mixture (75 mol% argon) and the liquid phase is ethanol. Note that droplets contain solid particles which fix their diameter.

The mass concentrations of the droplet phase and the plasma gas phase are, respectively, defined as $\rho_p = M_p/V_m$ and $\rho = M_g/V_m$. With these definitions, the ratio of mass flow rates of the droplet phase to the plasma gas phase is written as

$$\frac{\dot{m}_p}{\dot{m}_g} = k, \tag{4}$$

where $k = \rho_p/\rho$.

This simplified model will consist of linearizing conservation equations for each phase exchanging mass and energy in order to obtain the frequency acoustic response of the vaporizing mixture, i.e. the response factor.

4.1.1. Response factor. Due to plasma convective heating, droplet temperature can increase, resulting in an increase in saturation vapour pressure and therefore in an increase in vaporized mass. Consequently, if acoustic pressure modifies convective heating flux, it will also affect the vaporization rate. If the vaporization rate is above its mean value when pressure is also above its mean value, the acoustic pressure is encouraged and sound amplification occurs, following the Rayleigh criterion previously mentioned. However, if the vaporization rate is above its mean value when pressure is below its mean value, the acoustic pressure will be damped and sound attenuation takes place.

The response factor, N, is defined by the HW model [13] as the integral value of such an energy (or mass) addition over a given period of time, t, in a finite volume, V, normalized by the magnitude of pressure perturbation:

$$N = \frac{\int_t \int_V q'(t, V) p'(t, V)\, \mathrm{d}V\, \mathrm{d}t}{\int_t \int_V (p'(t, V))^2\, \mathrm{d}V\, \mathrm{d}t}, \tag{5}$$

where q' and p' are, respectively, the energy (or mass) and pressure perturbations, and are non-dimensional quantities. Note that the non-dimensional perturbed quantities, x, will be defined as $x' = (x - x_0)/x_0$, where x_0 is the unperturbed (mean) value of x.

In the following, we will assume a sinusoidal variation for q' and p' with the same period and that q' and p' are uniform over a finite volume. The response factor is then written [13]:

$$N = \frac{q'_{max}}{p'_{max}} \cos\theta, \tag{6}$$

where $p'(t) = p'_{max} \sin(\omega t)$ and $q(t) = q'_{max} \sin(\omega t + \theta)$.

Complex variations of implied quantities will be used. The response factor N^* will then be a complex function; consequently, we will calculate $N(\omega) = \bar{N} \cos\theta$, where ω, $\bar{N}$ and θ are, respectively, the angular frequency of the acoustic perturbation, the modulus of the response factor and its angle.

When the frequency response is positive, acoustic amplification occurs and when negative, attenuation dominates.

4.1.2. Assumptions.

- The droplet phase and the plasma gas phase are assumed to be continuous and their properties are uniform. Only the time dependence of properties is taken into account.
- Mass and energy transfers due to vaporization between the two phases are considered in a quasi-steady state. Energy transfers from the plasma gas are assumed to be mainly convective, radiation is not considered. Moreover, momentum transfers are not taken into account because velocity measurements performed by Bisson *et al* [17] have shown that products resulting from the suspension jet fragmentation (droplets and particles) follow plasma fluctuations. This means that the velocity of these products rapidly reaches the plasma gas velocity with a characteristic time of about 2×10^{-5} s for micrometre particles (see [18]). The influence of the momentum transfer is therefore expected to be out of range of the frequency of interest, i.e. above 50 kHz.
  This implies that the Reynolds number is low ($\ll 1$).
- Energy transfers and vaporization rate are unchanged during vaporization
- Droplets are assumed to be spherical, rigid, uniform in temperature and changes in diameter are negligible during one period of pressure oscillation.
- Specific heats and mean densities of both phases and vaporization latent heat are only dependent on mean temperatures. They are considered constant when linearizing equations.
- Diffusion coefficient D_v through the boundary layer of vaporizing droplets depends mainly on pressure such as $D_\mathrm{v} = C/p$, where C is constant and p is pressure.

4.1.3. Mass and energy equations. We consider the continuity and internal energy equations for the plasma gas phase and the droplet phase. Only retaining the time variations, these equations are written as follows [14]:

Plasma phase:

$$\frac{\partial \rho}{\partial t} = w, \tag{7}$$

$$\rho c_p \frac{\partial T}{\partial t} - \frac{\partial p}{\partial t} = -Q_v + w\left(c_\ell T_\mathrm{p} - \frac{p}{\rho_\ell} - c_p T\right), \tag{8}$$

Droplet phase:

$$\frac{\partial \rho_\mathrm{p}}{\partial t} = -w, \tag{9}$$

$$\rho_\mathrm{p} c_\ell \frac{\partial T_\mathrm{p}}{\partial t} = Q_v - w L_\mathrm{v}, \tag{10}$$

where T and T_p are, respectively, the temperature of the plasma phase and the droplet phase. w is the vaporization rate (droplet mass vaporized per time and volume units) and Q_v is the power exchanged by unit volume between the plasma phase and the droplet phase. c_p, c_ℓ and L_v are, respectively, the specific heats at constant pressure of the plasma and liquid (ethanol), and the latent heat of vaporization.

Equations (7) and (9) show the variations of mass concentrations of both phases due to vaporization. Equation (9) is not useful because $k = \rho_\mathrm{p}/\rho$. Equation (8) corresponds to the internal energy conservation and the second term of the left-hand side gives the variation of internal energy of plasma gas due to vaporization. The term p/ρ_ℓ is negligible with respect to the term $c_p T$.

The HW model takes into account only (9) and (10), i.e. a single phase, and considers a uniform and steady heating gas.

The vaporization rate is written according to [19] as

$$w = N_\mathrm{p} \pi d \rho \mathrm{D_v}\, Sh\, \ln\left(\frac{p}{p - p_\mathrm{v}}\right), \tag{11}$$

where Sh is the Sherwood number ($Sh = 2$ in the frame of present assumptions), p_v is the saturation vapour pressure of liquid and is given by the Clapeyron relationship as shown below.

Heat transfer exchanged per time and volume units, Q_v, is written as follows:

$$Q_v = N_\mathrm{p} \pi d \kappa\, N_u\, (T - T_\mathrm{p}), \tag{12}$$

where κ is the plasma thermal conductivity and N_u the Nusselt number ($N_u = 2$ in the frame of present assumptions).

In the following, the droplet temperature T_p will be neglected with respect to the plasma temperature T in equation (12).

Plasma heats the droplet phase. Temperature, T_p, of the latter increases, which imposes the saturation vapour pressure p_v. The vaporization rate is then driven by the difference of the ambient pressure, p, and p_v.

4.1.4. Linearized equations and response factor. Equations (7), (8), (10)–(12) are linearized following $x' = (x - x_0)/x_0$, where x is ρ, T, T_p, w, Q_v, p and p_v. ρ_p is linked to ρ through $k = \rho_\mathrm{p}/\rho$. After the identification of the unperturbed and first-order perturbed terms and the neglect of terms such as $x' \partial x_0/\partial t$, we obtain

$$\tau_\mathrm{v} \frac{\partial \rho'}{\partial t} = w', \tag{13}$$

$$\lambda \tau_\mathrm{v} \frac{\partial T'}{\partial t} - \tau_\mathrm{d} \frac{\partial p'}{\partial t} = \lambda_\mathrm{p} T_\mathrm{p}' - (1 + \lambda) T' + \frac{\Delta h_0}{L_\mathrm{v}} w', \tag{14}$$

$$k \lambda_\mathrm{p} \tau_\mathrm{v} \frac{\partial T_\mathrm{p}'}{\partial t} = T' - w', \tag{15}$$

where

$$\tau_\mathrm{v} = \frac{\rho_0}{w_0}, \tag{16}$$

$$\tau_\mathrm{d} = \frac{p_0}{L_\mathrm{v} \rho_0} \tau_\mathrm{v}, \tag{17}$$

$$\lambda = \frac{c_p T_0}{L_\mathrm{v}}, \tag{18}$$

$$\lambda_\mathrm{p} = \frac{c_\ell T_{p0}}{L_\mathrm{v}}, \tag{19}$$

$$\Delta h_0 = c_\ell T_{p0} - c_p T_0. \tag{20}$$

Table 3. Ethanol properties after [20].

Temperature T (K)	300
Density (kg m^{-3})	800
Specific heat (J kg^{-1} K^{-1})	2434
Latent heat of vaporization (J kg^{-1})	$L_v = D\exp\left(-\alpha\frac{T}{T_C}\right)\left(1-\frac{T}{T_C}\right)^{\beta}$
	$D = 50.43\times10^3$ (J kg^{-1})
	$\alpha = -0.4475$
	$\beta = 0.4989$
	$T_C = 513.9$ (K)
Saturation vapour pressure (bar)	$\log_{10}(p_v) = A - \frac{B}{T+C}$
	$A = 5.246\,77$
	$B = 1598.673$ (K)
	$C = -46.464$ (K)

In equations (11) and (12), the following linearizations of Q_v and w are used, where the unperturbed quantities follow $Q_{v0} = w_0 L_v$. This means that the main heat supplied to the droplet phase is consumed for vaporization in the unperturbed state. The choice for the Sherwood and Nusselt numbers has a weak influence in such circumstances (see equations (11) and (12)). The dimensionless perturbed quantities are

$$Q'_v = T', \tag{21}$$

$$w' = \rho' + \beta p'_v - (\beta+1)p', \tag{22}$$

where

$$\beta = \frac{p_{v0}}{(p_0 - p_{v0})\ln\left(\frac{p_0}{p_0 - p_{v0}}\right)}. \tag{23}$$

In equation (22), the saturation vapour pressure depends only upon the droplet temperature and p'_v can be derived as a function of T'_p by using the Clapeyron relationship:

$$\ln(p_v) = A - \frac{B}{T_p + C}, \tag{24}$$

where A, B and C are constants given by [20] for ethanol (table 3).

After linearization, we obtain

$$p'_v = bT'_p, \tag{25}$$

where

$$b = \frac{BT_{p0}}{(T_{p0}+C)^2}. \tag{26}$$

Considering complex notation ($e^{j\omega t}$) and assuming sinusoidal variation for ρ', T', T'_p and p', equations can be combined to obtain the complex response frequency ratio $N^*(\omega) = w'/p'$.

The perturbed temperature T' from equation (14) is inserted in equation (15) to obtain T'_p. The latter is introduced into equation (22) to obtain $N^*(\omega) = w'/p'$ by using equations (13), (22) and (25). We obtain, with $y = j\omega\tau_v$,

$$N^*(y) = \left(\frac{f-g}{\Delta}\right)(y), \tag{27}$$

whose real part corresponds to equation (6) and where

$$f(y) = \frac{\tau_d}{\tau_v}y + \frac{\beta+1}{\beta b}\lambda_p, \tag{28}$$

$$g(y) = \frac{k(\beta+1)\lambda_p}{\beta b}y(1+\lambda+\lambda y), \tag{29}$$

$$\Delta(y) = \frac{g(y)}{(\beta+1)y}\left[y + \frac{\beta b}{k\lambda_p} - 1\right] - \frac{\lambda_p}{\beta b y}(y-1) - \frac{\Delta h_0}{L_v}. \tag{30}$$

Thermo-physical properties for ethanol are taken from [20] and gathered in table 3.

4.2. Interpretation of acoustical amplification and attenuation

Figure 9 shows the response factor $N(\omega\tau_v)$ for a mean plasma temperature $T = 5000$ K and a mass flow rate ratio $k = 0.28$ as a function of dimensionless time $\omega\tau_v$.

Below $\omega\tau_v = 35$, the response factor is positive, which means acoustic amplification occurs, and above, sound attenuation dominates. The sign of the response factor is ruled by the dominant terms in equations (28) and (29). In figure 9, we also present the positive and negative contributions to $N(\omega\tau_v)$, respectively, corresponding to f/Δ and g/Δ.

When $\omega\tau_v < 10$, i.e. when the pressure variations are slow compared to the characteristic time of vaporization rate, the droplet temperature can follow changes imposed by heat flow (equation (21)) which depends on gas temperature ruled by equation (14). The increase in pressure above its mean value improves heat transfers from the plasma to the droplet. This results in an increase in droplet temperature and consequently vapour pressure. The vaporization rate increases due to the term $\ln(p/(p-p_v))$. Vaporization is therefore favoured when the acoustic pressure is above its mean value and acoustic amplification occurs. The term f/Δ shows this contribution.

When $\omega\tau_v \gg 1$, the droplet temperature cannot follow changes in heat transfers due to acoustic pressure and remains constant. The quadratic term y^2 in g/Δ dominates at high frequencies. Consequently, the increase in pressure above its mean value does not favour vaporization and instead tends to

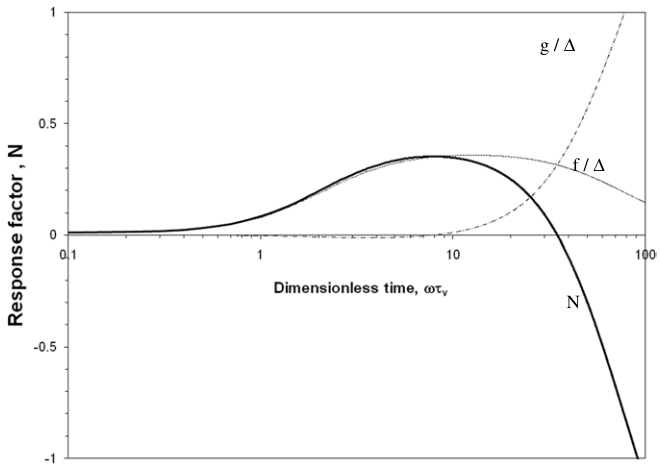

Figure 9. Frequency response N of a vaporizing ethanol droplet and its different contributions (see equations (27)–(29)); $T = 5000$ K, $\tau_v = 1.3 \times 10^{-4}$ s, $k = 0.28$.

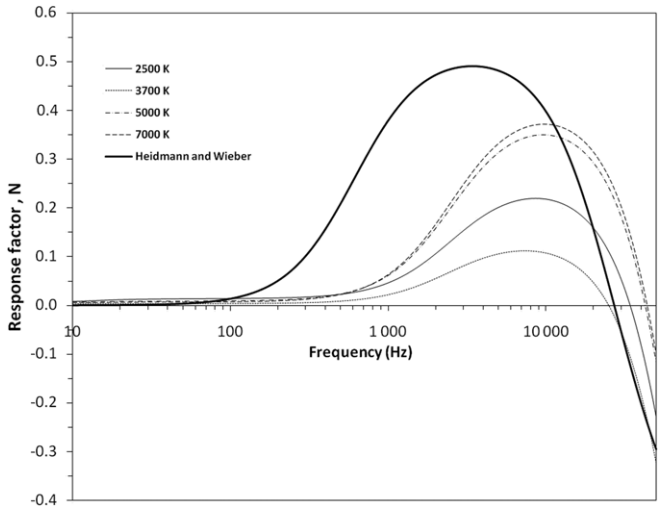

Figure 10. Frequency response of a vaporizing ethanol droplet following the Heidmann and Wieber model [13] and from this study for different plasma temperatures—$\tau_v = 1.3 \times 10^{-4}$ s, $k = 0.28$.

suppress it due to the term $\ln(p/(p - p_v))$. However, when the acoustic pressure is below its mean value, vaporization is encouraged due to the pressure difference. The net effect is that vaporization occurs when acoustic pressure is below its mean value. In this case, acoustic attenuation takes place. The β-value accounts for the pressure difference between the acoustic pressure and the vapour pressure.

Figure 10 shows the frequency response of a vaporizing ethanol droplet phase after the Heidmann and Wieber model and this study for $\tau_v = 1.3 \times 10^{-4}$ s for different plasma temperature values. The τ_v value is chosen to fit the experimental results and this value is consistent with previous evaluations [3]. The acoustic response in the HW model shows amplification and attenuation of acoustic emission over a wide frequency band. However, when considering the simplified mass and energy equations of plasma, the positive frequency response presents a better agreement in frequency with the experimental results. As shown in figure 8, plasma density and specific heat strongly vary, which produces non-monotonic variations of amplitude in frequency response. The frequency

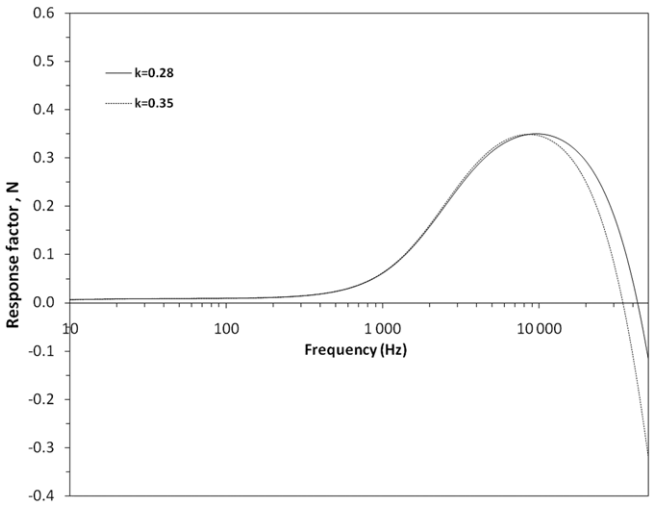

Figure 11. Frequency response of a vaporizing ethanol phase in an Ar–H_2 (75 mol% Ar) plasma for different values of parameter k—$\tau_v = 1.3 \times 10^{-4}$ s, $T = 5000$ K.

position of the positive response is weakly dependent on plasma temperature.

Figure 11 shows the dependence of frequency response on k. The k-values are calculated as the ratio of suspension mass flow rates (at 0.4 and 0.6 MPa, see table 2) and that of plasma gas (table 1). The change in k only affects the high frequency response because equation (15) shows that the increase in k is equivalent to the increase in the mean vaporization time τ_v. Consequently, the increase in k shifts the response factor to lower frequencies and increases the term g/Δ (equation (29)). However, experimental results show that the acoustic response seems to be independent of the change in pressure injection, which implies an increase in the suspension mass flow rate. This is probably because the increase in the suspension mass flow rate improves the local plasma cooling (see section 3.2) and modifies plasma gas density and specific heat.

In the experimental study in figure 7, we have observed that the transition between the amplification and the attenuation regions is shifted to lower frequencies when using pure argon instead of Ar–H_2 plasma. It is well known that thermal transfers are much more efficient in Ar–H_2 than in pure argon. Consequently, the characteristic time of vaporization τ_v is lower for argon than for Ar–H_2 and it can be expected that the amplification and attenuation regions are shifted towards lower frequencies when using pure argon.

5. Conclusion

SPS makes it possible to produce finely structured coatings with intermediate thicknesses (2–50 μm) for a large number of promising potential applications. The reproducibility of the coating properties depends to a large extent upon the control of the suspension injection within the plasma jet and the plasma stability. This is because the fragmentation and vaporization processes of droplets within the plasma govern the solid particles trajectories. Consequently, since the conventional particle diagnostic techniques are either not suited or difficult to

install, it is of interest to propose the on-line control techniques to monitor the suspension injection.

In this paper, we studied the frequency acoustic response of the suspension/plasma jet interaction. The analysis of experimental acoustic records produced by a dc plasma torch with and without suspension injection was performed. It was shown that the recorded sound follows the Fitaire law, i.e. the acoustic signal is proportional to the derivative of the arc torch voltage at a fixed arc current. Moreover, by studying the power spectrum of the torch voltage, it was observed that the latter is affected by the suspension injection at the nozzle exit. This implies that the suspension/plasma interaction produces a mechanical perturbation which propagates upstream within the torch. As shown in [10], since the dc plasma torch can behave like an acoustic resonator, this mechanical perturbation can participate in the excitation of the resonator. This is possible because the flow is subsonic.

The study of cross-correlation functions of the torch voltage and acoustic signals showed that the propagating time from the plasma to the microphone is dependent upon the suspension mass flow rate. It was interpreted in terms of local cooling of the plasma resulting in a decrease in sound velocity. A larger microphone frequency bandwidth should enhance the temporal resolution of such a measurement. The use of these propagating times could be used to control injection since the values of these times are directly linked to thermal transfers. The width of the density probability of the propagation times could be helpful in monitoring the stability of suspension/plasma interaction.

The spectral analysis of acoustic signals highlighted the frequency domains of sound amplification and attenuation. A simplified two-phase model of a vaporizing droplet immersed within a plasma jet allowed us to qualitatively interpret these phenomena which are dependent upon the dynamics of heat transfers from the plasma to the droplets. The frequency domains are linked to the mean vaporization time. Since the latter depends upon the square of the droplet diameter and the plasma properties (thermal conductivity and Nusselt number), the spectral study of acoustic emission could be used to monitor the stability of the fragmentation processes and also of thermal transfers.

The proposed acoustic method (cross-correlation between voltage and microphone or spectral study) should allow the monitoring of any deviations from chosen optimal deposition conditions. Indeed, this method gives an overall signature of the interaction between plasma and liquid suspension. These deviations could find their origins in instabilities of the liquid jet or slow drift of energetic performances of the plasma torch due to electrode erosion.

If an acoustic diagnostic technique is established from the present results, a frequency band should be selected either from 10 to 20 kHz (sound amplification) or from 35 to 50 kHz (sound attenuation). Frequencies below 10 kHz do not seem to be important in the acoustic process which is a signature of the interaction.

References

[1] Fauchais P, Etchart-Salas R, Rat V, Coudert J F, Caron N and Wittmann-Ténèze K 2008 *J. Therm. Spray Technol.* **17** 31–59

[2] Etchart-Salas R, Rat V, Coudert J F, Fauchais P and Lafougère G 2006 *J. High Temp. Mater. Process.* **10** 407–18

[3] Fazilleau J, Delbos C, Rat V, Coudert J F, Fauchais P and Pateyron B 2006 *Plasma Chem. Plasma Process.* **26** 371–91

[4] Fitaire M and Mantei T D 1972 *Phys. Fluids* **15** 464–9

[5] Dadgar H 1977 Acoustic emission in electric arc *PhD Thesis* University of Paris (in French)

[6] Pauvit R, de Izarra C and Vallée O 1997 *J. Physique III France* **7** 1561–70 (in French)

[7] Badie J M, Bresson J, Daïf A and Granier B 1996 *J. Physique III France* **6** 1423–33 (in French)

[8] Rat V and Coudert J F 2006 *J. Phys. D: Appl. Phys.* **39** 4799–807

[9] Morse P M and Ingard K U 1968 *Theoretical Acoustics* (Princeton, NJ: Princeton University Press)

[10] Coudert J F and Rat V 2008 *J. Phys. D: Appl. Phys.* **41** 205208

[11] Coudert J F, Rat V and Rigot D 2007 *J. Phys. D: Appl. Phys.* **40** 7357–66

[12] Kavka T, Kupke T and Arnold J 2007 Minimization of negative influence of electrode wear on generated plasma in dc arc torches *Proc. 18th Int. Symp. on Plasma Chemistry (Kyoto, Japan, 26–31 August 2007)* electronic file

[13] Heidmann M F and Wieber P R 1966 Analysis of frequency response characteristics of propellant vaporization *NASA* TM X-52195

[14] Dupays J and Vuillot F 2002 *J. Propulsion Power* **18** 222–4

[15] Rayleigh J W S 1945 *The Theory of Sound* vol II (New York: Dover)

[16] Pateyron B and Delluc G 1986 software TTWinner, ADEP—banque de données de l'Université et du CNRS Ed. Direction des Bibliothèques, des Musées et de l'Information Scientifique et technique and http://ttwinner.free.fr

[17] Bisson J F, Lamontagne M and Moreau C 2001 Ensemble in-flight particle diagnostics under thermal spray conditions *Thermal Spray: New Surfaces for New Millenium* ed C Berndt *et al* (Materials Park, OH: ASM International) pp 705–14

[18] Delbos C, Fazilleau J, Rat V, Coudert J F, Fauchais P and Pateyron B 2006 *Plasma Chem. Plasma Process.* **26** 393–414

[19] Lefebvre A H 1989 *Atomization and Sprays* (New York: Taylor and Francis)

[20] http://webbook.nist.gov/chemistry/